Geomechanics and Engineering, *Vol. 30, No. 2 (2022) 153-167*
https://doi.org/10.12989/gae.2022.30.2.153

Simulation study on porosity disturbance of ultra-large-diameter jet borehole excavation based on water jet coal wetting and softening model

Yan L. Guo[1], Hai B. Liu*[1], Jian Chen[2], Li W. Guo[2] and Hao M. Li[3]

[1]*School of Management, China University of Mining and Technology（Beijing）, Beijing, 100083, China*
[2]*College of Mining Engineering, North China University of Science and Technology, Tangshan, 063210, China*
[3]*College of Engineering, Huazhong Agricultural University, Wuhan, Hubei, China*

(Received June 21, 2021, Revised May 9, 2022, Accepted June 7, 2022)

Abstract. This study proposes a method to analyze the distribution of coal porosity disturbances after the excavation of ultra-large-diameter water jet boreholes using a coal wetting and softening model. The high-pressure jet is regarded as a short-term high-pressure water injection process. The water injection range is the coal softening range. The time when the reference point of the borehole wall is shocked by the high-pressure water column is equivalent to the time of high-pressure water injection of the coal wall. The influence of roadway excavation with support and borehole diameter on the ultra-large-diameter jet drilling excavation is also studied. The coal core around the borehole is used to measure the gas permeability for determining the porosity disturbance distribution of the coal in the sampling plane to verify the correctness of the simulation results. Results show that the excavation borehole is beneficial to the expansion of the roadway excavation disturbance, and the expansion distance of the roadway excavation disturbance has a quadratic relationship with the borehole diameter. Wetting and softening of the coal around the borehole wall will promote the uniform distribution of the overall porosity disturbance and reduce the amplitude of disturbance fluctuations.

Keywords: coal wetting and softening model; gas permeability; high pressure water jet; porosity disturbance distribution; roadway support; ultra-large-diameter borehole

1. Introduction

High-pressure water jet punching is a technology of pressure relief and gas permeability increase for coal seams (Latchoumi *et al.* 2019, Kong *et al.* 2016). Ordinary high-pressure water jet technology (Ren *et al.* 2020) for coal mines has small punching borehole diameter and large shock water resistance (Chen *et al.* 2018). A new high-pressure water jet technology that can excavate ultra-large-diameter boreholes has been developed to solve the abovementioned problems.

When water jet excavates boreholes of different diameters, the effective shock water column length remains unchanged, and gradual reaming is realized by changing the overall eccentric angle of the nozzle. The punching eccentric angles of the nozzle are 10°, 20°, and 30°. Thus, three jet drilling holes with diameters of 10–20, 20–40, and 40–60 mm are formed.

Notably, field operations can only be matched to the range of extraction disturbances by tentatively changing the punching aperture, because of the lack of theoretical guidance on the disturbance distribution of ultra-large-diameter jet borehole excavation. Doing so increases the workload and waste resources, which can obviously limit the method's application. Therefore, the coal disturbance law must be studied after the excavation of ultra-large-diameter boreholes.

Analysis of the current research status of coal excavation shows that scholars have established different mechanics (Komurlu *et al.* 2016), damage theories (Simpson *et al.* 2001), and physical models (Hao and Azzam 2005) to explain the excavation process. The distribution of seepage and disturbance area after rock excavation has also been investigated. The development of computer technology has facilitated research on large-scale model excavation and numerical simulation. The current simulations for studying excavation disturbances use the discrete element (DFM) (Salimzadeh *et al.* 2019), finite element method (FEM) (Zhao *et al.* 2020), anisotropic elastic method (Qi *et al.*, 2018), discrete element method (DEM) (Duan *et al.* 2018), cyclic dynamics theory method (Chen *et al.* 2019), rigid spring method (Kim *et al.* 2020), and SPH–FEM (Zhao *et al.* 2019, Wang *et al.* 2020) to simulate the excavation process. Among them, DFM, SPH–FEM, and DEM are mostly used to analyze shock damage of water particles. FEM method, anisotropic elastic method, cyclic dynamics theory method, and rigid spring method are effective for studying mechanics and damage disturbance.

The FEM method is simple and produces accurate simulation results; thus, it is suitable for coal seam excavation, support, coal softening, and elastoplastic changes (Yue *et al.* 2019, Cui *et al.* 2017). The water jet borehole excavation process will disturb the coal body

*Corresponding author, Professor
E-mail: hbliu@cumtb.edu.cn

ISSN: 2005-307X (Print), 2092-6219 (Online)

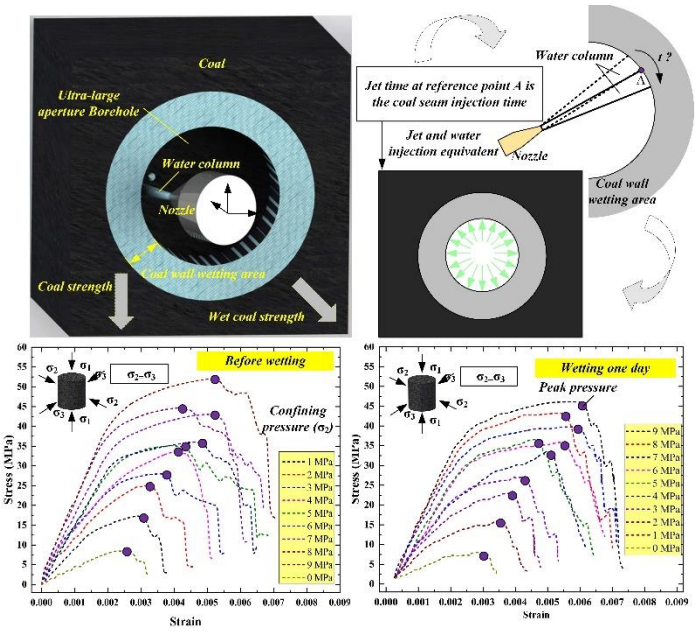

Fig. 1 Excavation model of jet drilling with ultra-large diameter

around the borehole wall to relieve pressure, thereby forming abundant seepage channels. The continuous shock of high-pressure water will result in the quick penetration of water into the coal. The strength of the coal that penetrates into the water will soften due to the long punching and reaming cycle of the entire working face (Wu *et al.* 2018), and this condition affects the distribution of the entire coal disturbance range. At present, scholars often ignore the softening effect of the coal around the borehole wall after wetting when studying water jet excavation; thus, inaccurate analysis results are generated. At the same time, the large change in borehole diameter and the support of the working face affect the distribution of disturbances (Zheng *et al.* 2019, Chen *et al.* 2020a). Therefore, studies on the change law of coal structure parameters after the softening of the borehole wall of jet borehole excavation in consideration of the large change in jet borehole diameter and bolt support are important.

This study aimed to determine the disturbance distribution law of coal structure parameters during the excavation of ultra-large-diameter jet borehole realistically and comprehensively. In this study, the water jet coal wetting and softening model is proposed to determine the seepage and wetting range of high-pressure water during the drilling process. The softening range of the coal body around the borehole is determined according to the law of coal strength after wetting. The pressure of the jet water column acting on the borehole wall is used as a bridge to establish the relationship between water jet and high-pressure water injection parameters. At the same time, finite element analysis software is used to solve the model, and the influence of the borehole diameter change and bolt support on the disturbance distribution is studied. Comparison with the disturbance law of porosity parameters obtained by measuring gas permeability through sampling around the jet borehole is conducted to verify the correctness of the simulation results. The relationship between the borehole diameter and the disturbance range of the maximum porosity parameter is analyzed, and the variation law of disturbance area and maximum disturbance radius at different locations is determined. As a result, a research experiment and a theoretical system based on the water jet coal wetting and softening model on the disturbance law of porosity parameters of ultra-large-diameter jet borehole excavation have been formed to provide support for efficient and safe on-site operations.

2. Excavation of ultra-large-diameter jet borehole based on water jet coal wetting and softening model

2.1 Water jet coal wetting and softening model

High-pressure water jets will cause the surrounding coal to become wet when the water column shocks the borehole wall. The triaxial mechanical compression failure test data after coal wetting (Liu *et al.* 2018) show that the coal body strength changes significantly (Lu *et al.* 2015) after coal wetting. As punching is completed within 1 day, the stress–strain curve of coal after 1 day of immersion is analyzed, as shown in Fig. 1. The change in the strength of coal around the borehole wall after wetting seriously affects the disturbance law of coal body excavation. Therefore, the softening characteristics of the coal body must be considered when studying the disturbance distribution of the porosity of jet borehole excavation to establish an ultra-large-diameter jet drilling model. When the jet water column shocks the borehole wall, high pressure will be formed on the coal wall of the borehole. The jet wetting process can be unified as a short-term coal wall water injection process to simplify the model. The water injection time is the time when the reference point A is shocked by the water column. The model derivation process proceeds as follows:

Assuming that the angular velocity of the overall rotation of the water jet nozzle is ω, the angle of rotation of the nozzle per unit time is

$$\alpha = \frac{180}{\pi}\omega \tag{1}$$

The divergence angle of the water column sprayed by the nozzle is β. At a reference point on the borehole wall, the continuous action time of the high-pressure water column is

$$t = \frac{\beta}{\alpha} \tag{2}$$

When water is injected from the borehole, the water pressure will cause the water to flow from the borehole wall into the fracture, and then the water will seep through the coal fracture network. The entire water injection process features constant pressure, and the effect of partial injection in the rotating process is the same as the effect of simultaneous injection. Regardless of the compressibility of the coal matrix and water and temperature transfer, the seepage process of fluid in fractures conforms to Darcy's law (Chen *et al.* 2020b).

$$v = \frac{k}{\mu}\frac{dP}{dr} \tag{3}$$

Then

$$Q = vA = 2\pi r \cdot \frac{k}{\mu}\frac{dP}{dr} \tag{4}$$

By separating the variables and integrating the abovementioned formula, we have

$$\int_{P_w}^{P_e} dP = \frac{Q\mu}{2\pi k} \cdot \int_{r_w}^{r_e} \frac{dr}{r} \tag{5}$$

The flow formula is

$$Q = 2\pi r \frac{P_w - P_e}{\mu \ln \dfrac{r_e}{r_w}} \tag{6}$$

During the analysis, the front edge of the seepage is in contact with air, the pressure is 0 MPa, and the velocity can be expressed as

$$v = \frac{kP_w}{r \ln \dfrac{r}{r_w}} \tag{7}$$

The micro element is used to determine the relationship between water injection time and water injection distance, as follows

$$vdt = dr \tag{8}$$

The differential expression of Formula (7) is

$$\frac{kP_w}{r \ln \dfrac{r}{r_w}} dt = dr \tag{9}$$

By integrating the aforementioned formula, we have

$$\int_0^t kP_w dt = \int_{r_w}^{r_e} r \ln \frac{r}{r_w} dr \tag{10}$$

$$\begin{aligned} kP_w t &= \int_{r_w}^{r_e} r \left(\ln r - \ln r_w\right) dr \\ &= \frac{1}{2} r_e^2 \left(\ln \frac{r_e}{r_w} - \frac{1}{2}\right) + \frac{1}{4} r_w^2 \end{aligned} \tag{11}$$

By introducing the equivalent high-pressure water injection time of the high-pressure water jet process into the abovementioned Formula (10), we have

$$kP_w \frac{\pi\beta}{180\omega} = \frac{1}{2} r_e^2 \left(\ln \frac{r_e}{r_w} - \frac{1}{2}\right) + \frac{1}{4} r_w^2 \tag{12}$$

The water pressure generated by the water column when the high-pressure water jet shocks the wall (Zhang and Zou 2018) is expressed as

$$P_w = 5.5\rho\left(u_0 \sqrt{\frac{b_0}{r_s}}\right)^2 \tag{13}$$

Introducing Formula (13) into Formula (12) yields

$$5.5k\rho\left(u_0 \sqrt{\frac{b_0}{r_s}}\right)^2 \frac{\pi\beta}{180\omega} = \frac{1}{2} r_e^2 \left(\ln \frac{r_e}{r_w} - \frac{1}{2}\right) + \frac{1}{4} r_w^2 \tag{14}$$

The relationship between the parameters of the high-pressure water jet and the wetting parameters of the coal body water injection seepage is established. The initial flow velocity, nozzle radius, and water column diffusion angle of the water jet are all proportional to the water injection wetting distance. By contrast, the rotation angular velocity of the water jet and the shock water column are inversely proportional to the water injection wetting distance.

The damage of coal after excavation adopts the extended DP criterion (exponential DP criterion). This criterion considers the intermediate principal stress and the effect of hydrostatic pressure on the yield of the material (Xu *et al.* 2019). The criterion can also reflect the dilatancy of coal. Therefore, the DP criterion can realistically represent the stress–strain relationship of coal during plastic deformation and failure. The exponential DP criterion can also directly import the test data into the parameters for analysis and produce realistic results. The principle of the exponential DP criterion is shown below.

The yield trajectory of the exponential DP criterion on the meridian is

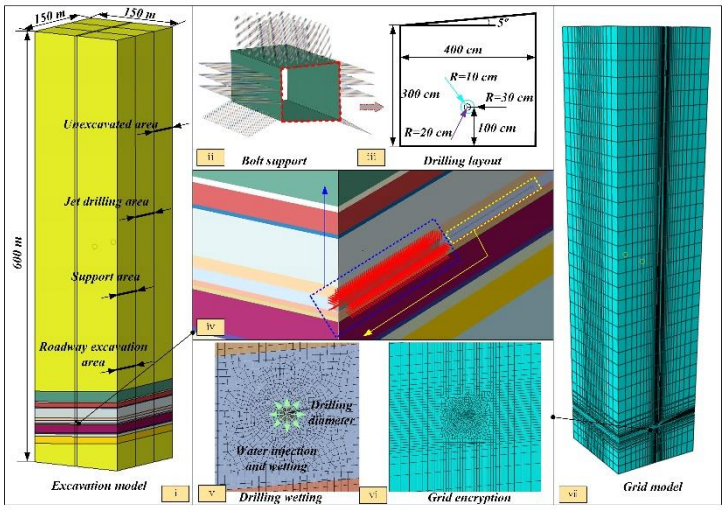

Fig. 2 Schematic of models

Table 1 Simulation parameters

Project	Density (10^3 kg/m^3)	Elastic modulus (GPa)	Poisson's ratio	Inclination (°)		
Siltstone	2480	28	0.21	5°		
Coal	1400	1	0.3	5°		
Brownish gray–dark gray siltstone	2200	18	0.23	5°		
Anchor	7800	200	0.2	Radius (m)	Length (m)	Support range (m)
				0.0125	3	50
Fluid injection	Water injection pressure (MPa)			Injection time (s)		
	6			6		

$$F=aq^b-p-p_t=0 \tag{15}$$

where a and b are the hardening parameters related to the material properties, and P_t is the material hardening parameter of the net water tensile and compressive strength. In this study, a and b are affected by the wetting and softening of coal.

P_t is related to the input test data as

$$P_t = a\sigma_c{}^b - \frac{\sigma_c}{3} \tag{16}$$

After the coal body of the borehole wall is wetted and softened, the damage of the entire coal body is divided into a softened area and a non-softened area. The softened area of the coal body is determined by r_e of water injection. The position is in the softened area when the distance between the analyzed position and the center point is less than r_e; the position is in the unsoftened area when the distance between the analyzed position and the center point is greater than r_e. The equation is

$$\begin{cases} a_0, b_0 & If \sqrt{(x-x_0)^2+(y-y_0)^2} \le r_e \\ a_1, b_1 & If \sqrt{(x-x_0)^2+(y-y_0)^2} > r_e \end{cases} \tag{17}$$

where a_0 and b_0 are the original strength parameters of coal body, and a_1 and b_1 are the strength parameters of coal body after softening. (x, y) is the coordinate of the analyzed position, and (x_0, y_0) is the coordinate of the center point of the borehole.

2.2 Simulation scheme and model parameters

The support of the working face has a certain influence on the disturbance of porosity parameters after excavation. Bolt support is prestressed support. In the current simulation process, the material strength of the working face is reduced, the bolt is activated, and the working face is excavated to realize the embedding of the anchor rod prestress. Field experience and literature indicate that the simulation results are similar to the field results when the modulus of the excavation area is reduced by 40% under the background of this working face (Zheng *et al.* 2019, Rehman *et al.* 2020, Lu *et al.* 2022). The model size and grid situation are shown in Fig. 2. The model size is 150 m×150 m×600 m, of which the roadway excavation sizes are set to 10 and 50 m. The underground test excavation borehole is 10 m, and the design of the excavation borehole for underground operation is 50 m. The drilling location is 1 m from the bottom plate on the center line of the working face. The shock aperture of high-pressure water jet

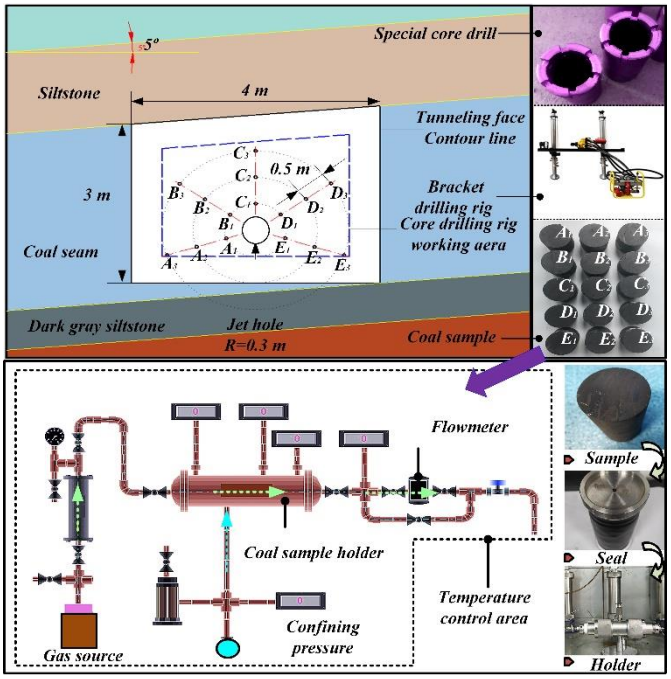

Fig. 3 Schematic of roadway face and MZY-1 coal seam permeability tester

excavation technology for ultra-large-diameter boreholes is from 15 cm to 60 cm. Thus, the simulated aperture is analyzed with a tolerance of 20 cm to ensure representativeness of the study. The selected apertures are 20, 40, and 60 cm. The water injection surface is the entire borehole wall. Bolt support is provided at the left and right sides and the roof position of the roadway. The top of the model is a free boundary, which is prepared for the in-situ stress balance analysis part, and the rest of the boundaries are displacement-fixed boundaries. All boundary hole pressures are 0 MPa. When dividing the grid, the stratigraphic grid adopts C3D8P type (An 8-node brick, trilinear displacement, trilinear pore pressure). The anchor rod adopts B31 type grid (A 2-node linear beam in space), which is the rod model. A total of 143,500 nodes and 134,304 elements are constructed in the stratum. The stratum is a solid domain, and the bolt is an embedded unit. Grid Analysis errors: 0 (0%), Analysis warnings: 2119 (1.5778%) meet the accuracy requirements of this article.

3. Confirmatory experiment

The void ratio (Feng *et al.* 2020, Wu *et al.* 2020) can characterize the degree of rock disturbance (de Figueiredo *et al.* 2017). Onsite sampling and laboratory measurement of gas permeability are conducted to determine the permeability distribution characteristics around the borehole to verify the correctness of the simulation method and the results. The experimental design aims to obtain the void ratio distribution around the borehole on the basis of the relationship between the permeability and the void ratio by measuring the gas permeability around the borehole. Sampling is performed after the punching operation is completed, as shown in Fig. 3.

The experimental punching depth is designed to be 10 m to reduce the difficulty of the experiment. The position of coal samples is finally determined to be 2 m at the front of the working surface to obtain effective coal samples and improve work efficiency. The sampling position is in the pressure relief area (Liu *et al.*, 2019; Wang and Cai, 2016), and the measured ground stress is 6 MPa. The obtained coal core is processed into a 50 mm×50 mm cylindrical experimental coal sample. The coal samples in five directions are labeled as $A_1A_2A_3$, $B_1B_2B_3$, $C_1C_2C_3$, $D_1D_2D_3$, and $E_1E_2E_3$. The samples are then dried at 80 °C for 24 h until analysis. The experimental scheme is described as follows. The length and diameter of the coal sample are measured after drying. The permeability of the coal seam is then measured at a constant temperature, surrounding rock pressure, and initial pressure by using a permeability meter.

The following parameters are set during the experiment to simulate the conditions of the underground coal seam: temperature of 24°C, surrounding rock pressure of 6 MPa, and initial gas pressure of 1.6 MPa. Changes in the permeability of the coal sample under different pressure can be calculated by recording the inlet and outlet gas pressures of the gripper and gas flow at the corresponding time. During the experiment, five groups of coal samples are separately tested. Prior to the experiment, the gas is percolated under a constant gas pressure for 1 h to adsorb the coal sample. During the experiment, 15 coal samples are measured separately, and the data are sorted into groups and analyzed. The permeability and void ratio distribution map of the working surface is obtained based on the change in infiltration and spatial relationship via an interpolation method. The method of mining cuttings around the borehole is carried out to determine the wetting distance of the coal wall at different apertures. The wetting ranges are 9.2, 9.8, and 10.4 cm.

The gas permeability in the coal sample is obtained by combining Formula (7), as shown below

$$k = \frac{200\,\mu Q_c P_c L}{A(P_1^{\,2} - P_2^{\,2})} \tag{17}$$

4. Results and discussion

4.1 Disturbance distribution of void ratio in excavation with different apertures based on wetting and softening model

The 3D void ratio distribution map around the borehole after excavation of jet boreholes with three different diameters is shown in Fig. 4.

The distribution of porosity disturbance range around each borehole is divided into three parts: the front cone, intermediate cylindrical, and tail peak areas. The softening of the coal body in the wetted area substantially increases the void ratio after stress equilibrium. The wetted area around the borehole also increases as the borehole diameter increases. The average values of the three wet thicknesses after simulation are 9.3, 9.8, and 10.2 cm, which are close to the experimental results. A large jet aperture corresponds to a large disturbance range at the same position from the working surface. When the drilling diameter is 20 cm, the difference between the maximum disturbance ranges of the tail peak area and intermediate cylindrical area is the largest. The tail peak area is affected by roadway and jet borehole excavations. The intermediate cylindrical area is a simple borehole excavation disturbance area. The radial influence ranges of the tail peak area and the middle cylindrical area around the borehole with a diameter of 40 cm are significantly increased. The difference between the two ranges decreases, and the length of the tail peak area increases significantly. The radial influence ranges of the tail peak area and the middle cylindrical area around the borehole with a diameter of 60 cm also significantly increase. At this time, the excavation and disturbance effects of the long, deep hole improve. The disturbance range is affected by the inclination angle of the coal seam, especially at positions near the contour plane of the roadway. The inclination angle of the disturbance distribution is similar to the inclination angle of the roadway contour line. Therefore, the coal seam inclination angle must be considered. The length of the tail peak area and the range of radial disturbance increase significantly as the borehole diameter of the jet increases when the section of the roadway is constant. The influence of roadway excavation disturbance is dominant when the borehole diameter is small. The disturbance caused by borehole excavation is dominant when the jet borehole diameter rises to 60 cm. Therefore, the disturbance effect of the large-aperture waterjet borehole is much better than that of the ordinary small-aperture waterjet borehole. The sizes of the radial disturbance range of the front cone area and the intermediate cylindrical area are mainly affected by the jet drilling aperture. Therefore, the jet drilling hole diameter can be selected depending on the work requirements. A jet borehole with a diameter of 40 cm is chosen when extracting CBM within the range of the tunneling working face to achieve safe and rapid mining. A jet borehole with a diameter of 60 cm is selected when CBM and coal resources should be efficiently recovered.

4.2 Distribution characteristics of void ratio after excavation of experimental section based on the relationship between porosity and permeability

The gas permeability data of each group of coal samples can be measured through triaxial permeability monitoring. Therefore, the laws of permeability change in all directions are analyzed. The change in coal permeability with gas pressure in five directions of A, B, C, D, and E is shown in Fig. 5.

The permeability of coal samples obtained in the directions of A, B, C, D, and E varies considerably. The gas permeability decreases with the increase in distance from the central drilling position under a constant gas pressure. When the coal seam gas pressure (i.e., the local gas pressure at the site) is 0.89 MPa, the coal permeability in each direction shows the order $K_C > K_B \approx K_D > K_A \approx K_E$. Thus, these findings imply that the coal seam fissure mostly develops in the direction of C, and the flow of gas in the larger pore fracture space increases the overall coal sample seepage flow. The regional permeability between C_1 and C_2 decreases rapidly, whereas that between C_2 and C_3 decreases slowly. The minimum permeability in direction C is the largest among those in other directions. Therefore, the range of fracture development in this direction exceeds the scope of C_3 monitoring. However, the development of coal body fractures is also large in oblique directions B and D. In general, the permeability first decreases rapidly and then decreases slowly as the distance from the center drilling increases. In the directions of A and E, the permeability is low and its change is different from that in the previous two groups (B and D). As the distance from the center drilling increases, the permeability first decreases slowly and then decreases rapidly. This phenomenon may be caused by the small disturbance range in the A and E directions of jet drilling. The fracture propagation distance in these directions is relatively short.

The permeability of the gas pressure at 0.89 MPa is extracted in all directions of A, B, C, D, and E. Contour lines are drawn to show the gas permeability distribution around the borehole to further analyze the experimental data. The void ratio distribution curve around the borehole is determined, as shown in Fig. 6, in accordance with the relationship between the permeability and the porosity. According to Casagrande's research (Keramatikerman *et al.* 2017, Gunaydin and Cetin 2020), the relationship between permeability and porosity is

$$K = 1.4K_{0.85}\psi^2 \tag{19}$$

Accordingly, the distribution law of the porosity around the borehole is obtained. The relationship between the permeability coefficient and permeability is

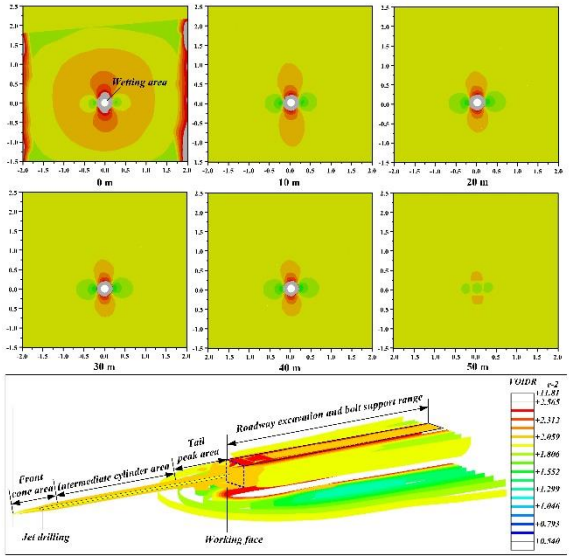

(a) 20 cm

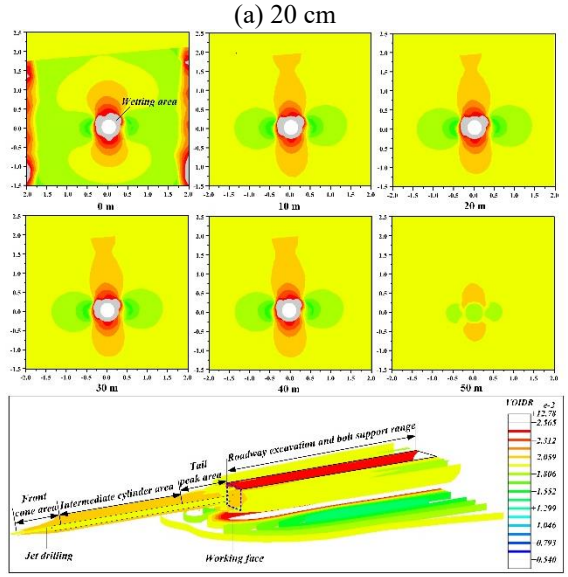

(b) 40 cm

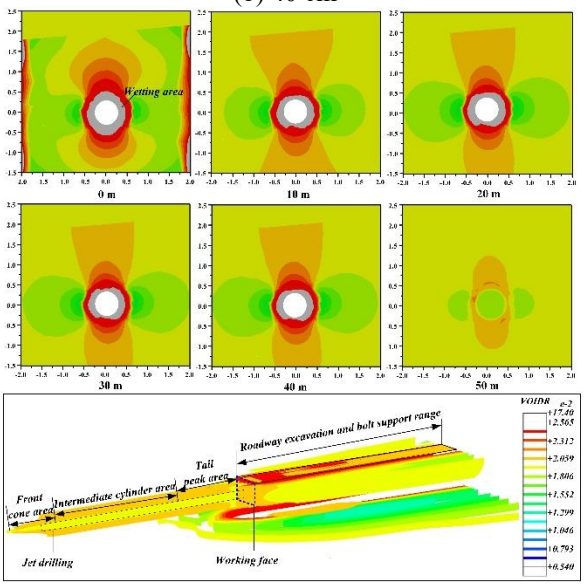

(c) 60 cm

Fig. 4 3D void ratio distribution map around the borehole after excavation of jet boreholes with three different diameters: (a) 20, (b) 40, and (c) 60 cm

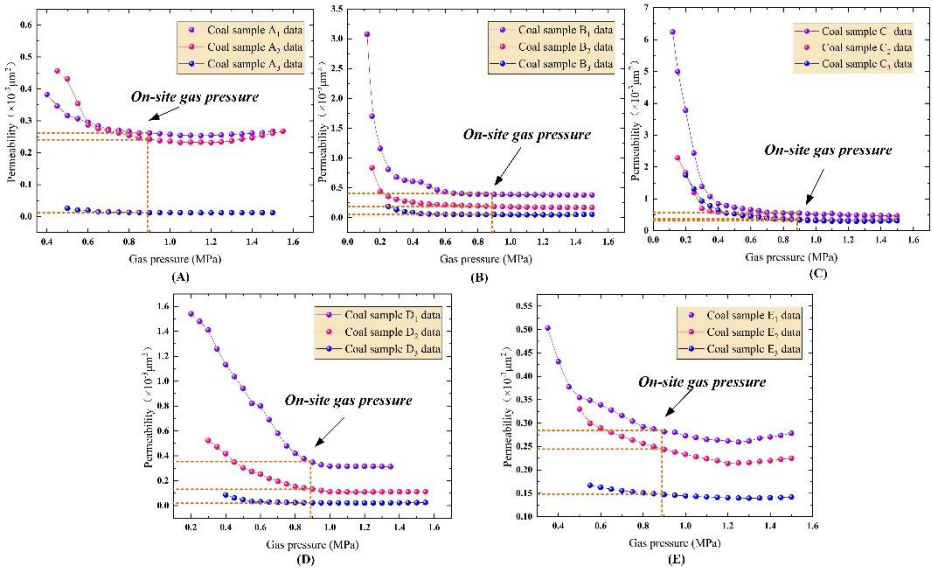

Fig. 5 Gas pressure–permeability change curve

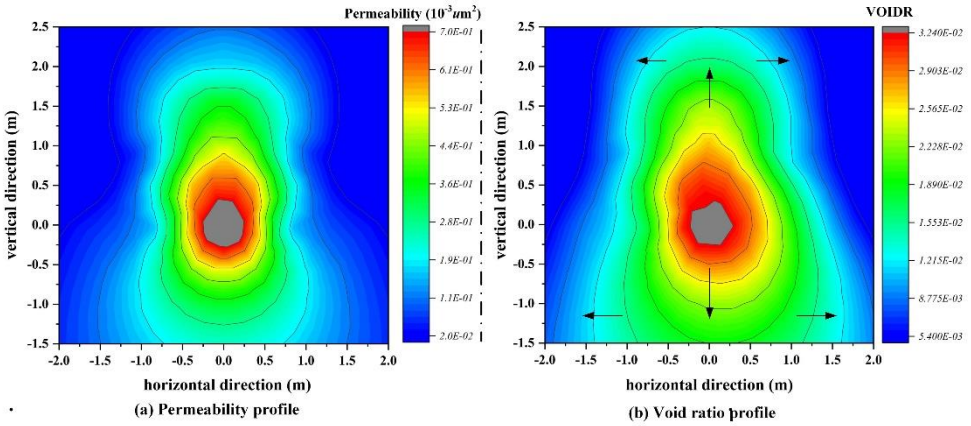

Fig. 6 Distribution of interface permeability and void ratio

$$K = \frac{k\gamma}{\mu} \tag{20}$$

The relationship between the permeability and porosity is

$$\frac{k\gamma}{\mu} = 1.4K_{0.85}\psi^2 \tag{21}$$

The relationship between void ratio and porosity is transformed into

$$\varepsilon_p = \frac{\psi}{1+\psi} \tag{22}$$

Introducing Formula (22) into Formula (21) yields

$$\frac{k\gamma}{\mu} = 1.4K_{0.85}\left(\frac{\varepsilon_p}{1-\varepsilon_p}\right)^2 \tag{23}$$

On the basis of this relationship, the void ratio distribution of coal around the borehole can be determined.

The measured permeability of the section mainly expands in the vertical direction, and the speed of permeability attenuation in this direction is slower than that in the horizontal direction. The high-permeability area in the upper part of the borehole is large because the fractures formed by the borehole excavation greatly contribute to gas seepage. This is due to the fact that the stress release degree of the upper part is larger than that of the lower part in the early stage of drilling excavation. The excavation disturbance range in the lower part of the borehole is obviously larger than that in the upper part of the borehole.

This is because the roof and both sides of the coal seam are supported by bolts, and no measures have been taken on the bottom plate. At the same time, the excavation position of the borehole is closer to the bottom plate, resulting in that the disturbance in the upper part of the borehole is not larger than that in the lower part of the borehole. The analysis of the VOIDR (void ratio) diagram indicates that the area affected by borehole excavation on coal seam pore

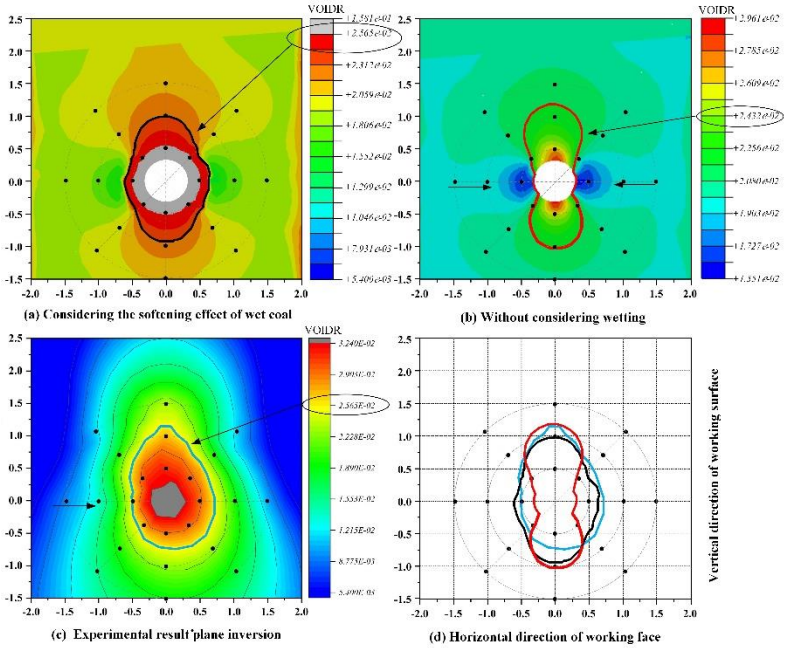

Fig. 7 Comparison of simulation and experimental results

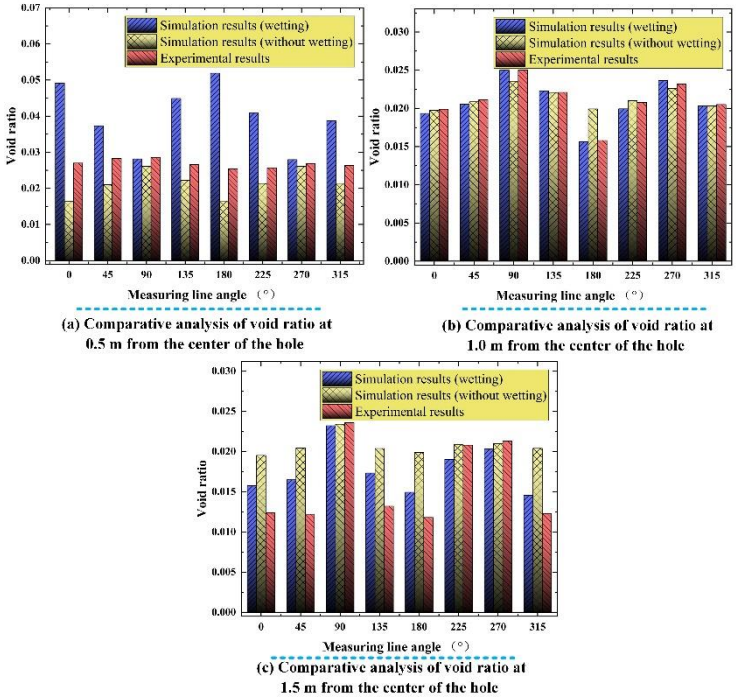

Fig. 8 Comparative analysis of simulation and experimental data

fracture density mainly presents a vertical ellipse, and the influence range extends to the entire roadway working face.

4.3 Quantitative verification of the accuracy of simulation results of different models

The simulation results of the disturbance (void ratio) distribution at 2 m are compared with the experimental findings (Fig. 7). The simulation results with and without wet coal are compared with the experimental results to verify the importance of coal softening in the wet area to the disturbance distribution. As observed, the contours of the high-value areas of the three void ratios are similar.

Fig. 7(b) does not consider the softening of the wetted area. The horizontal disturbance range is obviously different from the experimental results. The research results that consider coal softening and wetting (Fig. 7(a))) are close to the experimental results. Therefore, coal body wetting and softening should be considered when studying roadway excavation. The maximum void ratio is distributed around

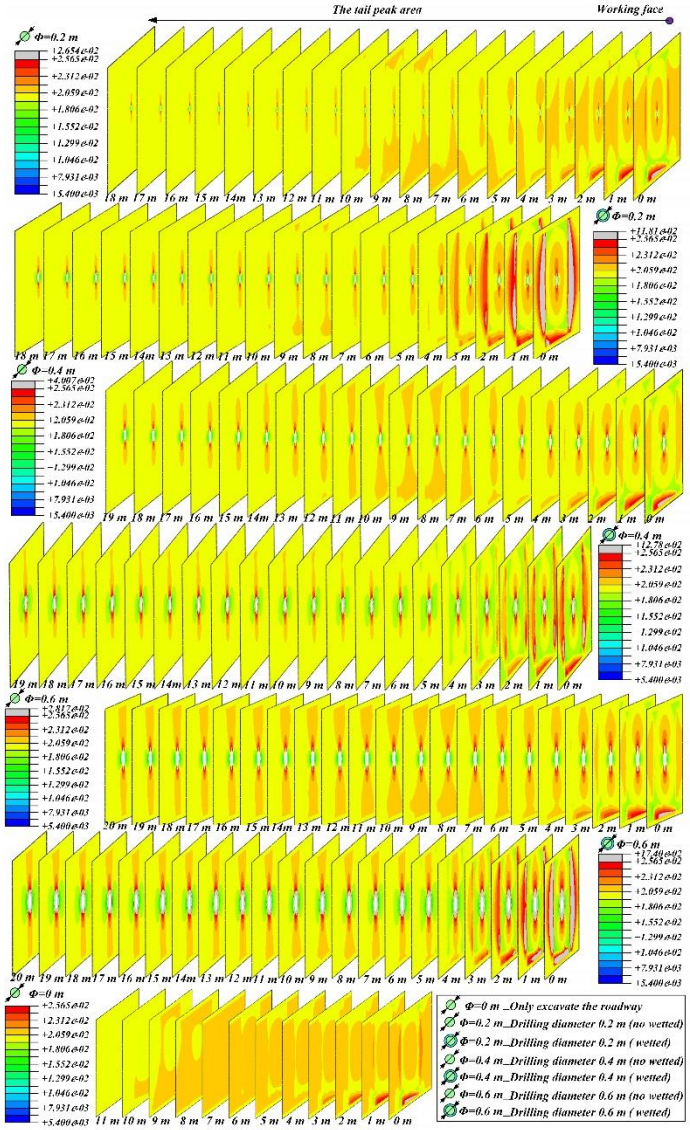

Fig. 9 Spatial distribution of disturbed superimposed areas after jet hole drilling with different apertures

the borehole, and the maximum values are 0.1581, 0.02961, and 0.03240 in sequence. The simulation results considering wetting are different from the experimental fitting results. The data fitted by the experiment are collected far from the borehole wall, which only avoids the coal-wetted area. Therefore, the experimental results have higher accuracy at a distance from the wall, while the simulation results at a closer position are more accurate. The simulation results considering the softening of the coal-wetted area are accurate. The data are collected and analyzed at a 45° interval with the center of the hole as the center to quantitatively determine the difference between the experimental and simulation results. The collected data are composed of data points at 0.5, 1, and 1.5 m from the hollow hole. A comparative analysis of the data is conducted, as shown in Fig. 8.

Figs. 8(a)-8(c) show the distribution of void ratios in different directions according to the data of 0.5, 1, and 1.5 m, respectively. At 0.5 m from the center of the borehole, the simulation results that consider wetting in all directions are relatively high, and the maximum difference is 0.027. At 1 and 1.5 m from the center of the borehole, the simulated and experimental results considering wetting are very close, and the maximum difference is 0.0035. This small difference indicates that the simulation results are very close to the experimental results from a quantitative perspective.

4.4 Influence of borehole diameter and coal softening range on the distribution of void ratio

The intermediate cylindrical area is the disturbance distribution area when excavating the jet borehole alone. The tail peak area is the distribution area of the superimposed disturbance of jet drilling and roadway excavation. The tail peak area is close to the working surface, and the disturbance distribution is complicated. Thus, in-depth analysis is required.

In the tail peak area, roadway excavation with support, borehole excavation, and wetting coal softening work together. The disturbance distribution at different locations in the tail

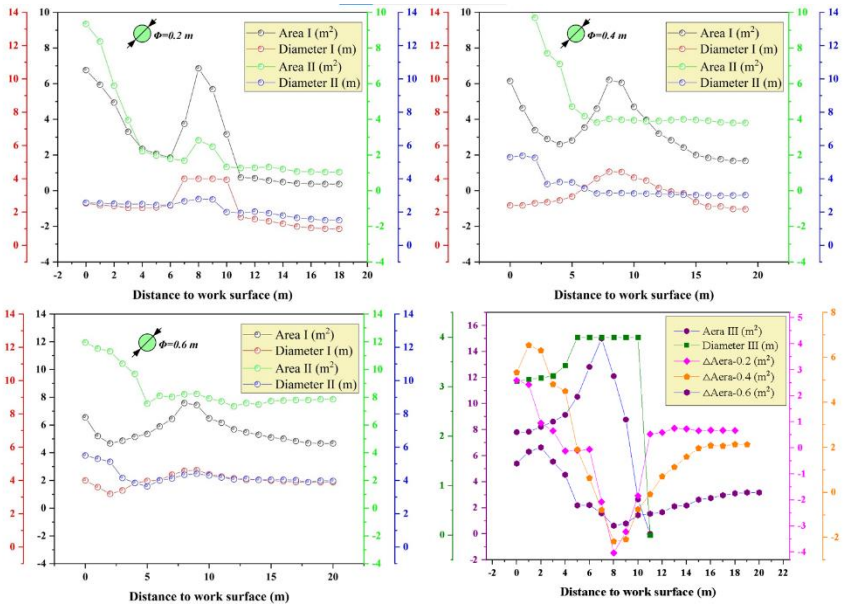

Fig. 10 Disturbance superimposed area parameter distribution curve after drilling with different apertures

peak area is sliced (Fig. 9) to verify the influence of the abovementioned factors on the disturbance distribution.

At a position close to the working surface, the range of the disturbance area is relatively large after the borehole is excavated. The disturbance area increases with the borehole diameter. When the hole diameter is the same, the disturbance area is large near the working surface and the void ratio is relatively high if coal wetting and softening are considered. The wetting and softening of coal can obviously increase the degree of disturbance in the plane. A comparison of the lengths of the tail peak area of each simulation result indicates that wetting and softening of the coal body can enhance the in-plane disturbance intensity, but they do not affect the superimposed axial disturbance propagation. Comparing the disturbance range of the front of the working face when only excavating the roadway without excavating the borehole implies that excavating the borehole can promote the expansion of the disturbance range of the roadway. Moreover, the axially superimposed disturbance range is related only to the diameter of the borehole excavation and not to the degree of wetting and softening. The disturbance caused by the excavation of ultra-large-diameter jet boreholes will superimpose the disturbance caused by the excavation of the roadway with supporting measures. The disturbance area and the maximum diameter of disturbance in the disturbance plane are analyzed, as shown in Fig. 10, to further quantitatively explore the change law of the tail peak area.

I represents the distribution curve of the disturbance area or maximum disturbance diameter of void ratio at different positions after the excavation of jet boreholes when the wetting and softening of coal are ignored; II represents the distribution curve of the disturbance area or maximum disturbance diameter of the void ratio at different positions after the excavation of jet drilling when the wetting and softening of coal are considered; III represents the distribution curve of the disturbance area or maximum disturbance diameter of void ratio at different locations when only supported roadways are excavated. The disturbance area and the maximum disturbance diameter decrease first, rebound, and decrease again as the distance from the working surface increases. When only the roadway is excavated, the area of the disturbance zone at the front end of the working face increases first and then decreases. Therefore, the increase in the area of the disturbance zone caused by the excavation of jet drilling is mainly due to the disturbance caused by the excavation of the roadway. At the same time, the magnitude of the increase in the intermediate rebound is related to whether wetting and softening are considered. When the coal body is wetted and softened, the increase in rebound area is relatively small. The softening of the wetted coal body will reduce the disturbance fluctuations and promote the uniform balance of the disturbance distribution. The softening of the wetted coal body does not affect the length of the urban superposition area when drilling holes of the same hole diameter. Thus, the simulation results that consider the softening of the wetted coal body will be different from those that ignore the softening of the wetted coal body. The softening of the wet coal causes disturbance changes. The disturbance caused by the softening of the wet coal body is opposite to the disturbance change caused by excavating the roadway only. Therefore, the softening of the wet coal body hinders the fluctuation change in the excavation disturbance of the roadway. The disturbed area and the distance from the working face under three types of excavation apertures are analyzed to quantitatively assess the disturbance law of borehole excavation considering the softening of wetted coal, as shown in Fig. 11.

$$\begin{aligned} y &= -0.0014x^3 + 0.0678x^2 - 1.0054x + 12.384, R^2 = 0.9204, \phi = 0.2\,m \\ y &= -0.004x^3 + 0.1622x^2 - 2.0935x + 12.454, R^2 = 0.9671, \phi = 0.4\,m \\ y &= -0.0056x^3 + 0.1974x^2 - 2.2236x + 9.4717, R^2 = 0.9386, \phi = 0.6\,m \end{aligned} \tag{24}$$

In the urban superposition area, the two present three relationships.

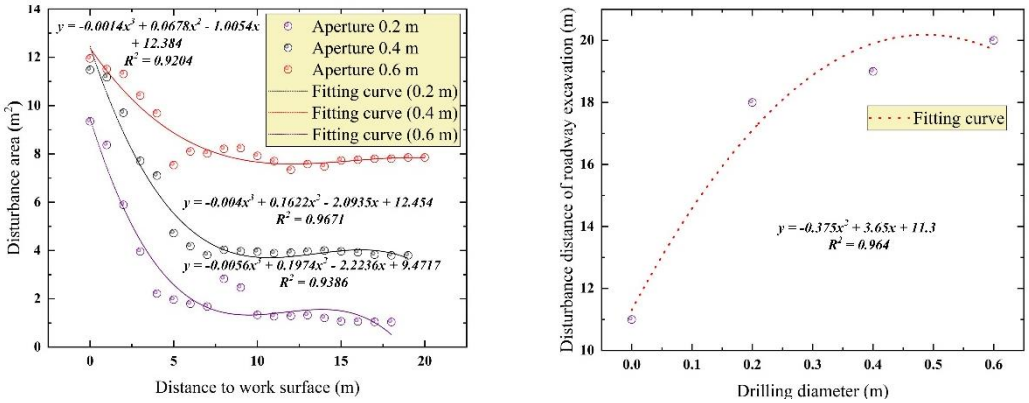

Fig. 11 Quantitative analysis diagram of drilling parameters and disturbance parameters

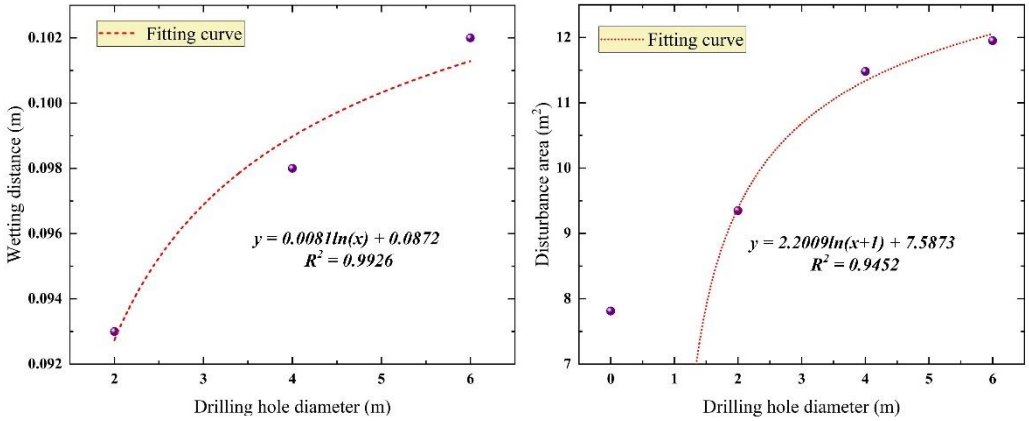

Fig. 12 Relation curve between drilling and disturbance parameters after excavation of working face

$$y = -0.375x^2 + 3.65x + 11.3, R^2 = 0.964 \quad (25)$$

The distribution state of the working surface directly affects the safety of workers. Therefore, the co-planar disturbance law is analyzed, as shown in Fig. 12.

The relationship equation between the water wetting distance and the porosity disturbance range area under different jet apertures is shown below

$$s + r = 0.0081\ln(d) + 2.2009\ln(d+1) + 7.6745 \quad (26)$$

4.5 Variation law of bolt support characteristics during excavation of jet boreholes with different diameters

Fig. 13 shows that the void ratio around the borehole changes significantly as the borehole diameter increases. When only the roadway is excavated without excavating the jet hole, the high-void disturbance area is mainly concentrated on both sides of the roadway, and the disturbance range is small. The middle of the working face presents a circular high-void area. When a jet hole with a diameter of 20 cm is excavated, the disturbance zone of the two sides of the roadway with high void ratio expands rapidly, and the maximum void ratio increases. The disturbance from the drilling of the borehole is superimposed on the two sides of the roadway. The area of high void ratio in the central area of the working face also changes significantly. The disturbance area of high void ratio around the borehole in the working face is gradually connected with the disturbance area of high void ratio near the roadway outline. When the borehole diameter of the excavated jet is 40 cm, the disturbance area of the two sides of the roadway with high void ratio changes slightly. However, the maximum void ratio increases significantly.

The high-void disturbance area around the borehole in the working face is fully connected to the high-void disturbance area near the roadway outline in the horizontal direction and vertically upward. When the borehole diameter of the excavated jet is 60 cm, the change in the disturbance area of the two sides of the roadway with high void ratio is small. However, the maximum void ratio increases significantly in this condition. The high-void disturbance area around the borehole in the working face is fully connected to the high-void disturbance area near the roadway outline. Therefore, whether excavating jet drilling greatly influences the size of the high-void area of the two sides of the roadway is unclear. After the jet borehole is excavated, the maximum void ratio of the two high-void areas of the roadway gradually increases as the borehole diameter of the jet borehole increases. Meanwhile, the range of the high-void area changes slightly. Therefore, the superposition of the disturbances on both sides of the roadway after excavation is the sum of the values of the

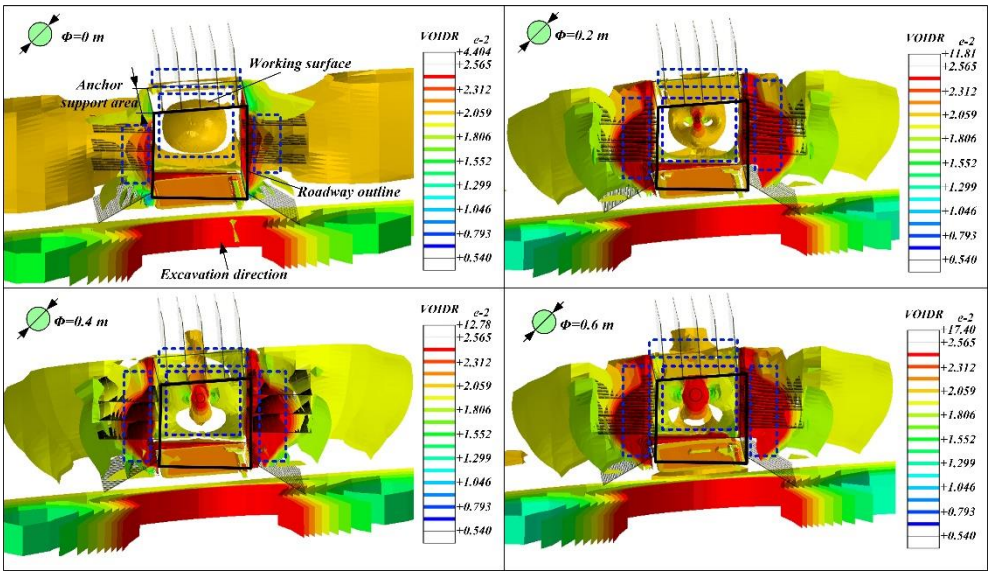

Fig. 13 Distribution of void ratio of roadway under multiple disturbances

roadway and borehole excavation disturbances. In the work area, the area around the borehole with high void ratio and the area around the roadway outline with high void ratio are gradually connected as the diameter of the excavated jet borehole increases. The increase in the bore diameter of the jet borehole increases the scope and degree of superposition of borehole and roadway excavation disturbances.

The relationship between the borehole diameter of excavation and the maximum disturbance void ratio of the two sides of the roadway is

$$y = -17.413x^2 + 30.427x + 4.9083, \quad R^2 = 0.9414 \quad (27)$$

The effect will be reduced when the hole diameter of the excavation exceeds 0.87. At this time, the disturbance of the two sides of the roadway begins to decrease.

5. Conclusions

- The softening effect of coal obvious influences the porosity disturbance. At the same hole diameter, the simulation results considering coal wetting and softening are large in the disturbance area near the working surface, and the void ratio is relatively high. Coal wetting and softening can obviously increase the degree of in-plane disturbance but do not obviously affect the axial disturbance propagation after superposition. The axially superimposed disturbance range is related to only the diameter of the borehole excavation and not to the degree of wetting and softening. The increase in disturbance area in the tail peak area is mainly caused by the distribution of disturbance of roadway excavation. The magnitude of the increase in the intermediate rebound is related to whether wetting and softening are considered. When the coal body is wetted and softened, the increase in rebound area is relatively small.
- The three-dimensional spatial distribution of coal porosity perturbed by the excavation of ultra-large-diameter jet boreholes is obtained. The distribution of the specific influence range of the void around each borehole is divided into three parts: the front cone, intermediate cylindrical, and tail peak areas. The disturbance area under excavation has a cubic relationship with the distance from the working face. The analysis of the situation of excavating only the roadway and not excavating the borehole indicates that excavating the borehole can promote the expansion of the excavation disturbance range of the roadway. At a position closer to the working face, the range of the disturbance area is relatively large after the borehole is excavated. The disturbance area also tends to increase as the borehole diameter increases.
- The disturbance produced by the excavation of ultra-large-diameter jet drilling will be superimposed with the disturbance produced by the excavation of the roadway with supporting measures. With the increase in the borehole diameter, the disturbance on the top of the roadway and the two supporting areas is enhanced, and the void ratio is significantly increased. The disturbance concentrates along the roof trapezoidal in the two sides of the roadway. The maximum disturbance of the two sides of the roadway also gradually increases with the increase in the drilling hole diameter within a certain range. A quadratic relationship exists between the borehole diameter of the excavation and the maximum disturbance void ratio of the two sides of the roadway. The fitting relationship equation indicates that the disturbance intensity of the two sides of the roadway decreases when the borehole diameter of the jet increases to 0.87 m.

Acknowledgments

This study was supported by the Central Guidance on Local Science and Technolog Development Fund of Hebei Province (226Z4601G), National Natural Science Foundation of China (52174182), Hebei Province Key R&D Program

(21376202D), Natural Science Foundation of Hebei Province (E2020209074).

References

Chen, J., Cheng, W. and Wang, G. (2020b), "Simulation of the meso-macro-scale fracture network development law of coal water injection based on a SEM reconstruction fracture COHESIVE model", *Fuel*, 119475. https://doi.org/10.1016/j.fuel.2020.119475.

Chen, J., Guo, L., Hu, Y. and Chen, Y. (2018), "Internal structure of a jet nozzle for coalbed methane mining based on airfoil curves", *J. Shock Vib*., **2018**. http://orcid.org/0000-0002-5043-9834.

Chen, J., Jiang, W., Wang, Q. and Zhang, Y. (2019), "Peridynamic analysis of drill-induced borehole damage", *Eng. Fail. Anal.*, **104**, 47-66. https://doi.org/10.1016/j.engfailanal.2019.05.028.

Chen, Z., Li, X., Dusseault, M.B. and Weng, L. (2020a), "Effect of excavation stress condition on hydraulic fracture behaviour", *Eng. Fract. Mech.* 106871. https://doi.org/10.1016/j.engfracmech.2020.106871.

Cui, L., Zheng, J.J., Dong, Y.K., Zhang, B. and Wang, A. (2017), "Prediction of critical strains and critical support pressures for circular tunnel excavated in strain-softening rock mass", *Eng. Geol.*, **224**, 43-61. https://doi.org/10.1016/j.enggeo.2017.04.022.

Duan, K., Wu, W. and Kwok, C.Y. (2018), "Discrete element modelling of stress-induced instability of directional drilling boreholes in anisotropic rock", *Tunn. Undergr. Sp. Tech.*, **81**, 55-67. https://doi.org/10.1016/j.tust.2018.07.001.

Feng, R., Balling, N. and Grana, D. (2020), "Lithofacies classification of a geothermal reservoir in Denmark and its facies-dependent porosity estimation from seismic inversion", *Geothermics*, **87**, 101854. https://doi.org/10.1016/j.geothermics.2020.101854.

de Figueiredo, L.P., Grana, D., Santos, M., Figueiredo, W., Roisenberg, M. and Neto, G.S. (2017), "Bayesian seismic inversion based on rock-physics prior modeling for the joint estimation of acoustic impedance, porosity and lithofacies", *J. Comput. Phys.*, **336**, 128-142. https://doi.org/10.1016/j.jcp.2017.02.013.

Gunaydin, O. and Cetin, H. (2020), "Determination of stress distribution on active fault by means of Casagrande method; an innovative approach", *Soil Dyn. Earthq. Eng.*, **129**, 105920. https://doi.org/10.1016/j.soildyn.2019.105920.

Hao, Y. and Azzam, R. (2005), "The plastic zones and displacements around underground openings in rock masses containing a fault", *Tunn. Undergr. Sp. Tech.*, **20**(1), 49-61. https://doi.org/10.1016/j.tust.2004.05.003.

Keramatikerman, M., Chegenizadeh, A. and Nikraz, H. (2017), "An investigation into effect of sawdust treatment on permeability and compressibility of soil-bentonite slurry cut-off wall", *J. Cleaner Production*, **162**, 1-6. https://doi.org/10.1016/j.jclepro.2017.05.160.

Kim, K., Rutqvist, J. and Birkholzer, J. (2020), "Lattice modeling of excavation damage in argillaceous clay formations: Influence of deformation and strength anisotropy", *Tunn. Undergr. Sp. Tech.*, **98**, 103196. https://doi.org/10.1016/j.tust.2019.103196.

Komurlu, E., Kesimal, A. and Demir, S. (2016), "Experimental and numerical analyses on determination of indirect (splitting) tensile strength of cemented paste backfill materials under different loading apparatus", *Geomech. Eng.*, **10**(6), 775-791. https://doi.org/10.12989/gae.2016.10.6.775.

Kong, X., Wang, E., Liu, X., Li, N., Chen, L., Feng, J., Kong, B., Li, D. and Liu, Q. (2016), "Coupled analysis about multi-factors to the effective influence radius of hydraulic flushing: application of response surface methodology", *J. Natural Gas Sci. Eng.*, **32**, 538-548. https://doi.org/10.1016/j.jngse.2016.04.043.

Latchoumi, T., Balamurugan, K., Dinesh, K. and Ezhilarasi, T. (2019), "Particle swarm optimization approach for waterjet cavitation peening", *Measurement*, **141**, 184-189. https://doi.org/10.1016/j.measurement.2019.04.040.

Liu, D., He, M. and Cai, M. (2018), "A damage model for modeling the complete stress–strain relations of brittle rocks under uniaxial compression", *Int. J. Damage Mech.*, **27**(7), 1000-1019. https://doi.org/10.1177/1056789517720804.

Lu, H., Gutierrez, M. and Kim, E. (2022), "Empirical approach for reliability evaluation of tunnel excavation stability using the Q rock mass classification system", *Undergr. Sp.*, 2467-9674, https://doi.org/10.1016/j.undsp.2022.01.001.

Liu, H., Lin, B. and Jiang, C. (2019), "A new method for determining coal seam permeability redistribution induced by roadway excavation and its applications", *Process Safety and Environmental Protection*, **131**, 1-8. https://doi.org/10.1016/j.psep.2019.08.019.

Lu, Y., Huang, F., Liu, X. and Ao, X. (2015), "On the failure pattern of sandstone impacted by high-velocity water jet", *Int. J. Impact Eng.*, **76**, 67-74. https://doi.org/10.1016/j.ijimpeng.2014.09.008.

Qi, D., Li, L. and Jiao, Y. (2018), "The stress state around an elliptical borehole in anisotropy medium", *J. Petroleum Sci. Eng.*, **166**, 313-323. https://doi.org/10.1016/j.petrol.2018.03.013.

Rehman, H., Naji, A.M., Ali, W., Junaid, M., Abdullah, R.A. and Yoo, H.K. (2020), "Numerical evaluation of new Austrian tunneling method excavation sequences: A case study", *Int. J. Min. Sci. Tech.*, **30**(3), 381-386. https://doi.org/10.1016/j.ijmst.2020.03.009.

Ren, F., Fang, T. and Cheng, X. (2020), "Study on rock damage and failure depth under particle water-jet coupling impact", *Int. J. Impact Eng.*, **139**, 103504. https://doi.org/10.1016/j.ijimpeng.2020.103504.

Salimzadeh, S., Grandahl, M., Medetbekova, M. and Nick, H. (2019), "A novel radial jet drilling stimulation technique for enhancing heat recovery from fractured geothermal reservoirs", *Renew. Energ.*, **139**, 395-409. https://doi.org/10.1016/j.renene.2019.02.073.

Simpson, G., Guéguen, Y. and Schneider, F. (2001), "Permeability enhancement due to microcrack dilatancy in the damage regime", *J. Geophys. Res. Solid Earth*, **106**(3), 3999-4016. https://doi.org/10.1029/2000JB900194.

Wang, X. and Cai, M. (2016), "FLAC/SPECFEM2D coupled numerical simulation of wavefields near excavation boundaries in underground mines", *Comput. Geosci.*, **96**, 147-158. https://doi.org/10.1016/j.cageo.2016.08.010.

Wang, X., Yuan, W., Yan, Y. and Zhang, X. (2020), "Scale effect of mechanical properties of jointed rock mass: a numerical study based on particle flow code", *Geomech. Eng.*, **21**(3), 259-268. https://doi.org/10.12989/gae.2020.21.3.259.

Wu, N., Liang, Z., Zhou, J. and Zhang, L. (2020), "Energy evolution characteristics of coal specimens with preformed holes under uniaxial compression", *Geomech. Eng.*, **20**(1), 55-66. https://doi.org/10.12989/gae.2020.20.1.055.

Wu, X., Jiang, Y. and Guan, Z. (2018), "A modified strain-softening model with multi-post-peak behaviours and its application in circular tunnel", *Eng. Geol.*, **240**, 21-33. https://doi.org/10.1016/j.enggeo.2018.03.031.

Xu, J., Zhou, R., Song, D., Li, N., Zhang, K. and Xi, D. (2019), "Deformation and damage dynamic characteristics of coal–rock materials in deep coal mines", *Int. J. Damage Mech.*, **28**, no. 1, 58-78. https://doi.org/10.1177/1056789517741950.

Yue, J., Wang, Z. and Chen, J. (2019), "Investigation of timing characteristics of the imbibition height of remolded coal without gas", *Energy Sources, Part A: Recovery, Utilization, and Environmental Effects*, **41**(2), 156-166. https://doi.org/10.1080/15567036.2018.1505980.

Zhao, Y., Lin, B., Liu, T., Kong, J. and Zheng, Y. (2020), "Gas flow in hydraulic slotting-disturbed coal seam considering stress relief induced damage", *J. Natural Gas Sci. Eng.*, 103160. https://doi.org/10.1016/j.jngse.2020.103160.

Zhang, Y. and Zou, Q. (2018), "A prediction model for the slot depth of high pressure water jet", *Results in Phys.*, **11**, 1105-1109. https://doi.org/10.1016/j.rinp.2018.11.020.

Zhao, J., Zhang, G., Xu, Y., Lin, A., Zhao, J. and Yang, D. (2019), "Enhancing rate of penetration in a tight formation with high-pressure water jet (HPWJ) via a downhole pressurized drilling tool", *J. Petroleum Sci. Eng.*, **174**, 1194-1207. https://doi.org/10.1016/j.petrol.2018.11.042.

Zheng, Y., Chen, C., Liu, T., Song, D. and Meng, F. (2019), "Stability analysis of anti-dip bedding rock slopes locally reinforced by rock bolts", *Eng. Geol.*, **251**, 228-240. https://doi.org/10.1016/j.enggeo.2019.02.002.

CC